

# Data-driven deep local imaging using both surface and borehole seismic data

Yi Liu\*, Norwegian University of Science and Technology; Joost van der Neut, Delft University of Technology; Børge Arntsen, Norwegian University of Science and Technology; Kees Wapenaar, Delft University of Technology

## SUMMARY

Seismic interferometry (SI) is a proven data-driven redatuming method to create virtual sources for better illumination of the target area. It requires a physical receiver at the position of the created virtual source. With the development of the iterative Marchenko method, one can now use surface data alone to create a virtual source in the subsurface, but an estimate of the direct wavefield from those virtual source positions to the surface is needed, which means an adequately accurate smooth velocity model is nevertheless necessary. We show that when borehole data from a horizontal well is available, one can combine the principles of SI and the Marchenko method to formulate several inversion-based redatuming schemes, such that no prior smooth velocity model is needed at all and that the exact forms of retrieving the reflection responses from above and from below can also be obtained. Furthermore, the internal multiples are accounted for using these exact forms. No surrounding acquisition geometry is required or multi-component well data is needed. We demonstrate the proposed schemes using a synthetic gas cloud example. We then show the retrieved responses and the migrated images using only a local velocity model. The results show that given the same velocity uncertainty, these responses that are redatumed by data produce a better positioned image near the well than a surface seismic image. The proposed schemes can be beneficial for deep boreholes and complex areas with big velocity uncertainties.

## INTRODUCTION

Different types of borehole seismic data (Schuster et al., 2004; Bakulin and Calvert, 2006; Vasconcelos and Snieder, 2008b; Poletto et al., 2010) have been used to create virtual source data by applying seismic interferometry (SI) (Wapenaar and Fokkema, 2006; Curtis et al., 2006). Compared to other redatuming methods, SI does not require any velocity information and the physical receivers are turned into virtual source (or vice versa). Known approaches to SI are crosscorrelation (CC) (Snieder, 2004), deconvolution (DC) (Vasconcelos and Snieder, 2008a), multidimensional deconvolution (MDD) (van der Neut et al., 2011) and crosscoherence (CH) (Nakata et al., 2011). Comprehensive and systematic comparisons among different approaches can be found in Wapenaar et al. (2011), Snieder et al. (2009), and Galetti and Curtis (2012).

Taking a step beyond SI, the iterative Marchenko method (Brogini et al., 2012; Wapenaar et al., 2013) has been developed to create virtual sources in the subsurface from surface seismic data alone, which means the presence of physical receivers at depth is no longer needed. Various applications that use the Marchenko method for imaging are suggested by Wapenaar et al. (2014). However, the scheme does require an estimate of the direct wavefield from the virtual source positions to the

surface, and the requirement on the accuracy of such estimate is yet to be studied.

We show that when the data from a horizontal borehole is available, the direct wavefield can be obtained directly from the borehole data, thus making the whole Marchenko imaging scheme completely independent of any traveltime estimation errors. Further, by combining the principles of SI and the properties of the focusing functions in the Marchenko method, the exact formulations of retrieving the reflection responses from above and from below the well can be obtained. The internal multiples can also be properly accounted for. Compared to the scheme for imaging from below by Poliannikov (2011), whose approach is based on source-receiver interferometry (SRI) (Curtis and Halliday, 2010), our scheme is an inversion-based scheme under one-sided illumination and can account for internal multiples. These schemes also do not require multicomponent borehole data, both for imaging from above (Mehta et al., 2007) and from below (van der Neut and Wapenaar, 2015), but the surface related multiples are assumed to have been removed from both surface and borehole datasets.

We start by introducing some of the properties of the focusing functions (Wapenaar et al., 2014). Then we use them to derive the equations for retrieving the reflection responses from above and from below, and suggest some approximations as alternatives for situations in which the focusing functions cannot be obtained. In total, we illustrate four schemes for imaging from above and two for imaging from below. We show the results using a synthetic gas cloud model.

## THEORY

### The focusing functions

The two focusing functions  $f_1^\pm(\mathbf{x}|\mathbf{x}'_i, t)$  and  $f_2^\pm(\mathbf{x}|\mathbf{x}''_0, t)$  have been studied in detail in Wapenaar et al. (2014). Here we will just show briefly some results.  $f_1^\pm(\mathbf{x}''_0|\mathbf{x}'_i, t)$  describes a wavefield that focuses at position  $\mathbf{x}'_i$  at depth level  $i$  and is recorded at position  $\mathbf{x}''_0$  at surface level 0, while  $f_2^\pm(\mathbf{x}'_i|\mathbf{x}''_0, t)$  describes a wavefield that focuses at position  $\mathbf{x}''_0$  and is recorded at position  $\mathbf{x}'_i$ . The superscripts  $+$  and  $-$  denote downgoing and upgoing, respectively. The two focusing functions are mutually related via

$$\widehat{f}_1^+(\mathbf{x}''_0|\mathbf{x}'_i) = \widehat{f}_2^-(\mathbf{x}'_i|\mathbf{x}''_0); \quad (1)$$

$$-\left(\widehat{f}_1^-(\mathbf{x}''_0|\mathbf{x}'_i)\right)^* = \widehat{f}_2^+(\mathbf{x}'_i|\mathbf{x}''_0), \quad (2)$$

where the focusing functions are now represented in the frequency domain, indicated by the  $\widehat{\phantom{x}}$  above (the angular frequency variable  $\omega$  is omitted), and the superscript  $*$  denotes the complex conjugate. Due of the causality arguments for the one-way Green's function  $G^-(\mathbf{x}'_i|\mathbf{x}''_0, t)$ ,  $G^+(\mathbf{x}'_i|\mathbf{x}''_0, t)$  and the focusing function  $f_2^+(\mathbf{x}'_i|\mathbf{x}''_0, t)$  (Wapenaar et al., 2014), the following relations apply, for  $t < t_d(\mathbf{x}'_i, \mathbf{x}''_0)$ , where  $t_d$  is the direct

## Data-driven imaging above and below a horizontal well

arrival time from  $\mathbf{x}_0''$  to  $\mathbf{x}'_i$ ,

$$f_1^-(\mathbf{x}_0''|\mathbf{x}'_i, t) = \int_{\partial D_0} \int_{-\infty}^t \mathcal{R}^{\cup}(\mathbf{x}_0''|\mathbf{x}_0, t-t') f_1^+(\mathbf{x}_0|\mathbf{x}'_i, t') dt' d\mathbf{x}_0; \quad (3)$$

$$f_1^+(\mathbf{x}_0''|\mathbf{x}'_i, -t) = \int_{\partial D_0} \int_{-\infty}^t \mathcal{R}^{\cup}(\mathbf{x}_0''|\mathbf{x}_0, t-t') f_1^-(\mathbf{x}_0|\mathbf{x}'_i, -t') dt' d\mathbf{x}_0; \quad (4)$$

and for  $t \geq t_d(\mathbf{x}'_i, \mathbf{x}_0'')$ ,

$$G^-(\mathbf{x}'_i|\mathbf{x}_0'', t) = \int_{\partial D_0} \int_{-\infty}^t \mathcal{R}^{\cup}(\mathbf{x}_0''|\mathbf{x}_0, t-t') f_1^+(\mathbf{x}_0|\mathbf{x}'_i, t') dt' d\mathbf{x}_0; \quad (5)$$

$$\begin{aligned} G^+(\mathbf{x}'_i|\mathbf{x}_0'', t) \\ = - \int_{\partial D_0} \int_{-\infty}^t \mathcal{R}^{\cup}(\mathbf{x}_0''|\mathbf{x}_0, t-t') f_1^-(\mathbf{x}_0|\mathbf{x}'_i, -t') dt' d\mathbf{x}_0 \\ + f_1^+(\mathbf{x}_0''|\mathbf{x}'_i, -t). \end{aligned} \quad (6)$$

Here  $\mathcal{R}^{\cup}(\mathbf{x}_0''|\mathbf{x}_0, t)$  can be viewed as the reflection response that one could obtain from surface seismic data after surface related multiple removal (SRME). This is to be distinguished from  $\hat{\mathcal{R}}^{\cup}(\mathbf{x}'_i|\mathbf{x}_i)$  in ‘‘Imaging from above’’, and  $\hat{\mathcal{R}}^{\cap}(\mathbf{x}'_i|\mathbf{x}_i)$  in ‘‘Imaging from below’’. The time window indicated by  $t_d(\mathbf{x}'_i, \mathbf{x}_0'')$  can for example be found by the direct arrivals from borehole data. In addition, the starting approximation to the focusing functions written in the frequency domain is

$$\hat{f}_{1,0}^+(\mathbf{x}_0''|\mathbf{x}'_i) = \hat{f}_{2,0}^-(\mathbf{x}'_i|\mathbf{x}_0'') = \hat{G}_d^*(\mathbf{x}'_i|\mathbf{x}_0''), \quad (7)$$

where the subscript  $_0$  indicates that the  $\hat{G}_d^*(\mathbf{x}'_i|\mathbf{x}_0'')$  is the initial estimate, the direct arrival of the Green’s function obtained from borehole data with a time gate.

### Image from above

To image from above, the idea is to retrieve the reflection response coming from the reflectors below the borehole level  $i$ , as if the medium above is reflection-free. Such a reflection response  $\hat{\mathcal{R}}^{\cup}(\mathbf{x}'_i|\mathbf{x}_i)$  can be found by the standard redatuming method of SI by MDD (Wapenaar and van der Neut, 2010)

$$\hat{G}^-(\mathbf{x}'_i|\mathbf{x}_0'') = \int_{\partial D_i} \hat{\mathcal{R}}^{\cup}(\mathbf{x}'_i|\mathbf{x}_i) \hat{G}^+(\mathbf{x}_i|\mathbf{x}_0'') d\mathbf{x}_i. \quad (8)$$

Here we treat  $\hat{G}^-(\mathbf{x}'_i|\mathbf{x}_0'')$  and  $\hat{G}^+(\mathbf{x}_i|\mathbf{x}_0'')$  as if they come from borehole data, not as solutions of the Marchenko method using only surface reflection data. This scheme requires up-down decomposition using multi-component data. Solving Eq. 8 by MDD, the retrieved  $\hat{\mathcal{R}}^{\cup}(\mathbf{x}'_i|\mathbf{x}_i)$  does not contain any downgoing reflections coming from above. When such separation is not available, one option is to replace the downgoing  $\hat{G}^+(\mathbf{x}_i|\mathbf{x}_0'')$  with the direct arrivals in the borehole data and use the remaining events as the upgoing  $\hat{G}^-(\mathbf{x}'_i|\mathbf{x}_0'')$  (Bakulin and Calvert, 2006), such as

$$\hat{G}^-(\mathbf{x}'_i|\mathbf{x}_0'') - \hat{G}_d^-(\mathbf{x}'_i|\mathbf{x}_0'') \approx \int_{\partial D_i} \hat{\mathcal{R}}^{\cup}(\mathbf{x}'_i|\mathbf{x}_i) \hat{G}_d^-(\mathbf{x}_i|\mathbf{x}_0'') d\mathbf{x}_i. \quad (9)$$

Here the retrieved  $\hat{\mathcal{R}}^{\cup}(\mathbf{x}'_i|\mathbf{x}_i)$  will contain some spurious events related to this wavefield separation approximation. Now, to

utilize the surface reflection response  $\hat{\mathcal{R}}^{\cup}(\mathbf{x}_0''|\mathbf{x}_0)$  as in the Marchenko method, we substitute Eq. 5 and 6 into Eq. 8 and can get

$$\begin{aligned} \mathcal{W}' \left[ \int_{\partial D_0} \hat{\mathcal{R}}^{\cup}(\mathbf{x}_0''|\mathbf{x}_0) \hat{f}_1^+(\mathbf{x}_0|\mathbf{x}'_i) d\mathbf{x}_0 \right] \\ = \int_{\partial D_i} \hat{\mathcal{R}}^{\cup}(\mathbf{x}'_i|\mathbf{x}_i) \times \\ \left\{ \mathcal{W}' \left[ \int_{\partial D_0} \hat{\mathcal{R}}^{\cup}(\mathbf{x}_0''|\mathbf{x}_0) \hat{f}_1^{*-}(\mathbf{x}_0|\mathbf{x}'_i) d\mathbf{x}_0 + \hat{f}_1^{*-}(\mathbf{x}_0''|\mathbf{x}'_i) \right] \right\} d\mathbf{x}_i. \end{aligned} \quad (10)$$

Here an operator  $\mathcal{W}'$  is introduced to represent the operation of inverse Fourier transforming the data, applying a time window which passes data only for  $t \geq t_d(\mathbf{x}'_i, \mathbf{x}_0'')$ , and Fourier transforming the result back to the frequency domain. Such retrieved  $\hat{\mathcal{R}}^{\cup}(\mathbf{x}'_i|\mathbf{x}_i)$  does not contain any spurious events related to the internal multiples from the overburden. To make a similar choice as for Eq. 9, we can also write another version of it by using Eq. 5, 7 on the left-hand side of Eq. 8 and replace  $\hat{G}^+(\mathbf{x}_i|\mathbf{x}_0'')$  with the direct arrivals in the borehole data  $G_d^*(\mathbf{x}'_i|\mathbf{x}_0)$  on the right-hand side, then Eq. 8 becomes

$$\begin{aligned} \mathcal{W}' \left[ \int_{\partial D_0} \hat{G}_d^*(\mathbf{x}'_i|\mathbf{x}_0) \hat{\mathcal{R}}^{\cup}(\mathbf{x}_0''|\mathbf{x}_0) d\mathbf{x}_0 \right] \\ \approx \int_{\partial D_i} \hat{\mathcal{R}}^{\cup}(\mathbf{x}'_i|\mathbf{x}_i) \hat{G}_d^-(\mathbf{x}_i|\mathbf{x}_0'') d\mathbf{x}_i. \end{aligned} \quad (11)$$

The retrieved response by this scheme will contain spurious events related to internal multiples, but much simpler to implement in practice. One more additional choice without much implication is to join Eq. 9 and 11 and solve with MDD, which reads in matrix forms as,

$$\begin{bmatrix} \mathbf{U}_1 \\ \alpha \mathbf{U}_2 \end{bmatrix} = \mathbf{R} \begin{bmatrix} \mathbf{D}_1 \\ \alpha \mathbf{D}_1 \end{bmatrix} \quad (12)$$

where  $\mathbf{U}_1$  and  $\mathbf{U}_2$  correspond to the left-hand sides of Eq. 9 and 11, and  $\mathbf{D}_1$  to the right-hand sides. Here  $\alpha$  is a user-defined frequency dependent scalar weight. Inverting this joint scheme might be better than inverting a single scheme (Eq. 9 or 11). First of all, both problems may have different frequency content and signal-to-noise ratios; second, the borehole data may have higher propagation angles that could help to image structures that could not be found in the surface data; third, the data could be incomplete, so merging them could help.

### Image from below

The concept of imaging from below means to retrieve the reflection response coming from the reflectors above the borehole level  $i$ , as if the medium underneath is reflection-free. Such a reflection response  $\hat{\mathcal{R}}^{\cap}(\mathbf{x}'_i|\mathbf{x}_i)$  is found to be related to the focusing function  $\hat{f}_2^-(\mathbf{x}'_i|\mathbf{x}_0'')$  via (Wapenaar et al., 2014)

$$\hat{f}_2^-(\mathbf{x}'_i|\mathbf{x}_0'') = \int_{\partial D_i} \hat{\mathcal{R}}^{\cap}(\mathbf{x}'_i|\mathbf{x}_i) \hat{f}_2^-(\mathbf{x}_i|\mathbf{x}_0'') d\mathbf{x}_i. \quad (13)$$

Now by using Eq. 2, and Eq. 3, Eq. 13 can be rewritten as

$$\begin{aligned} - \left\{ \mathcal{W} \left[ \int_{\partial D_0} \hat{f}_1^+(\mathbf{x}_0|\mathbf{x}'_i) \hat{\mathcal{R}}^{\cup}(\mathbf{x}_0''|\mathbf{x}_0) d\mathbf{x} \right] \right\}^* \\ = \int_{\partial D_i} \hat{\mathcal{R}}^{\cap}(\mathbf{x}'_i|\mathbf{x}_i) \hat{f}_2^-(\mathbf{x}_i|\mathbf{x}_0'') d\mathbf{x}_i. \end{aligned} \quad (14)$$

## Data-driven imaging above and below a horizontal well

Here the operator  $\mathcal{W}$  is defined to represent the operation of inverse Fourier transforming the data, applying a time window which passes data only for  $t < t_d(\mathbf{x}'_i, \mathbf{x}''_0)$ , and Fourier transforming the result back to the frequency domain.  $\hat{f}_1^+(\mathbf{x}''_0|\mathbf{x}_i)$  needs to be calculated from the Marchenko method with the input of  $\hat{\mathcal{R}}^\cup(\mathbf{x}''_0|\mathbf{x}_0)$  and the direct arrivals  $\hat{G}_d^*(\mathbf{x}_i|\mathbf{x}''_0)$ . Similar to the case from above, a simple approximation to the above equation is

$$-\left\{ \mathcal{W} \left[ \int_{\partial D_0} \hat{G}_d^*(\mathbf{x}'_i|\mathbf{x}_0) \hat{\mathcal{R}}^\cup(\mathbf{x}''_0|\mathbf{x}_0) d\mathbf{x} \right] \right\}^* \approx \int_{\partial D_i} \hat{\mathcal{R}}^\cap(\mathbf{x}'_i|\mathbf{x}_i) \hat{G}_d^*(\mathbf{x}_i|\mathbf{x}''_0) d\mathbf{x}_i, \quad (15)$$

where we used Eq. 7 for substitution. A correlation-based approximate solution to this equation is closely related to the method by Poliannikov (2011), whose derivation is based on SRI, but we solve it here by inversion instead. We see now that because of the substitution of Eq. 7, solving Eq. 15 either by MDD or by CC results in some spurious events in the retrieved  $\hat{\mathcal{R}}^\cap(\mathbf{x}'_i|\mathbf{x}_i)$ , and those spurious events related to the upgoing internal multiples can be removed by using Eq. 14. However, when the internal multiples are not strong, Eq. 15 offers a simple but sufficient alternative. Next, we show some synthetic results.

### SYNTHETIC EXAMPLE

We illustrate the schemes using a synthetic acoustic model. The model is 5 by 5.5 km with a grid sampling of 2.5 m, shown in Fig. 1. Both the borehole data and the surface data are modeled using a finite difference method (Thorbecke and Draganov, 2011) without a free surface. The borehole data have 201 sources at the surface and 81 receivers at 3.7 km depth. The surface data have 201 sources and receivers at the surface.

To image from above, four schemes (Eq. 9, 11, 10 and 12) are tested, and the retrieved virtual reflection responses (in red) are compared with the reference response (in blue) in Fig. 2. The reference response is modeled with a homogeneous overburden. The reference source position is  $x_1 = 2500, x_3 = 3700$  (indicated by the green dot in Fig. 1), and the receiver positions are from  $x_1 = 1500$  to  $x_1 = 3500$  at the same depth. For the first scheme (Eq. 9), only the borehole data are used; for the second scheme (Eq. 11), the surface reflection responses are used to redatum the direct arrivals from the borehole data; for the third scheme (Eq. 10), the input is the same as for the second scheme, but an iterative Marchenko method (Wapenaar et al., 2014) is used to find the focusing functions, where the traveltimes and the initial focusing functions (time-gated direct arrivals) are taken directly from the borehole data; for the fourth scheme (Eq. 12), scheme one and two are joined and the focusing functions are not computed. Fig. 4 shows the corresponding migrated images. By comparing the traces in Fig. 2, it is observed that panel a) has the most spurious events, but mainly for the later arrivals (all events after 1 s are added an extra scalar gain), whereas these downgoing events are almost completely removed in panel c). This is because the up-down

wavefields are properly decomposed by the focusing functions. If the correct focusing functions are difficult to find, one can use the fourth scheme. This joint scheme could reserve higher propagation angles and also helps to merge two datasets with different signal-to-noise ratios.

To image from below, two schemes (Eq. 15 and 14) are tested, and the retrieved virtual reflection responses (in red) are compared with the reference response (in blue) in Fig. 3. Here the reference response is modeled with a homogeneous underburden. An extra scalar gain is added on all events after 3 s. In the trace comparison, one can see that the second scheme using the focusing functions results in a better match in terms of the amplitude and less spurious events. Nevertheless, the first scheme recovers the main reflectors phase well and can be more easily implemented in practice.

To show that these schemes are particularly suitable when there is uncertainty in the velocity model, a smooth velocity model is tried for migration. The comparison is shown in Fig. 6. In panel a), the image from above and from below are put together to form a local image. The retrieved responses in Fig. 2 d) and Fig. 3 b) are used for these local images. By comparison, we see that the local image are much more resilient to velocity uncertainties in the model. Also, it is noticed that the same reflector is mapped to different positions in the two images, so a further application of these imaging results could be to exploit this sensitivity to velocity errors to form a better constrained inversion scheme for velocities.

### CONCLUSIONS

We present several inversion-based schemes for deep local imaging above and below a horizontal well. The redatuming schemes are completely data-driven, meaning no estimate of direct wavefield or velocity model is needed. For imaging, only a local velocity model is needed. The methods extend previous approaches to include surface data, and offer accurate methods for retrieving the reflection responses that do not require surrounding source boundaries. Furthermore, internal multiples can be properly accounted for using single-component borehole data and surface data. The synthetic example shows promising results for more robust deep imaging in the presence of velocity uncertainties. The extension to include non-horizontal boreholes, and surface related multiples remains to be studied.

### ACKNOWLEDGEMENTS

The authors acknowledge the Research Council of Norway, ConocoPhillips, Det norske oljeselskap, Statoil, Talisman, TOTAL and Wintershall for financing the work through the research centre DrillWell. In addition, the ROSE consortium at NTNU is acknowledged. We also thank Jan Thorbecke at TU Delft for the help on the Marchenko method.

## Data-driven imaging above and below a horizontal well

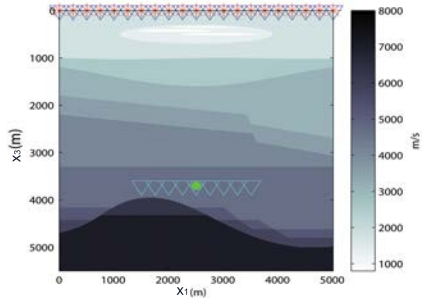


Figure 1: P-wave velocity model and datasets geometries. The stars denote sources and the triangles denote receivers. The green dot indicates the position of the reference shot.

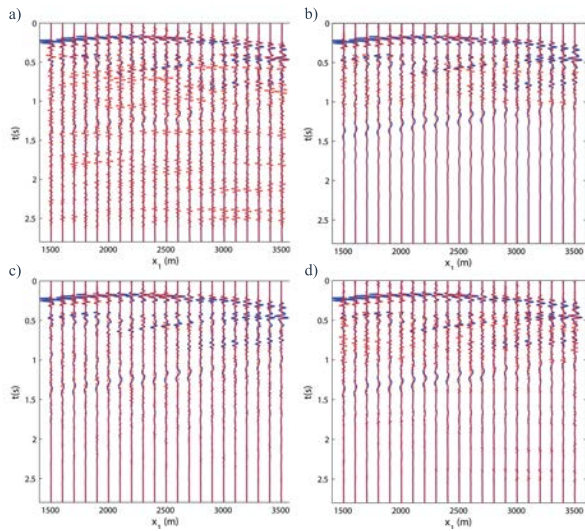


Figure 2: Reflection responses from above. Trace comparison between the retrieved responses (in red) and the reference responses (in blue), using a) Eq. 9, b) Eq. 11, c) Eq. 10 and d) Eq. 12. The reference source position is  $x_1 = 2500, x_3 = 3700$ , and the receivers are at the same depth as the source.

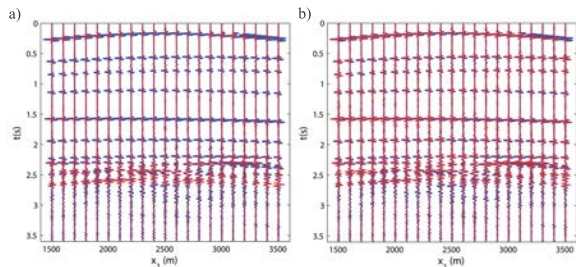


Figure 3: Reflection responses from below. Trace comparison between the retrieved responses (red) and the reference responses (blue), using a) Eq. 15, b) Eq. 14. The reference source position is  $x_1 = 2500, x_3 = 3700$ , and the receivers are at the same depth as the source.

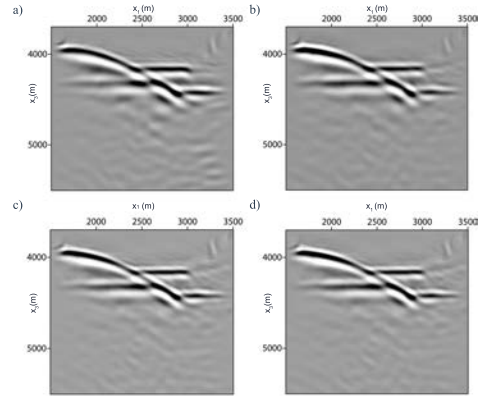


Figure 4: Migrated images from above using the retrieved responses from the counterpart in Fig. 2. A true local velocity model of the target zone is used.

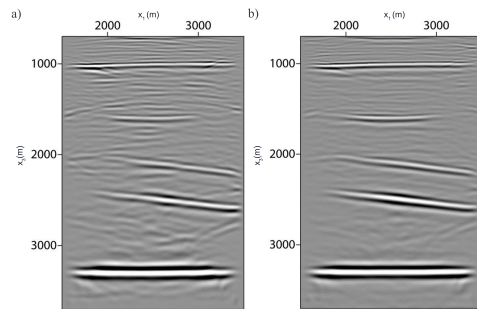


Figure 5: Migrated images from below using the retrieved responses as shown in Fig. 3. A true local velocity model of the imaged zone is used.

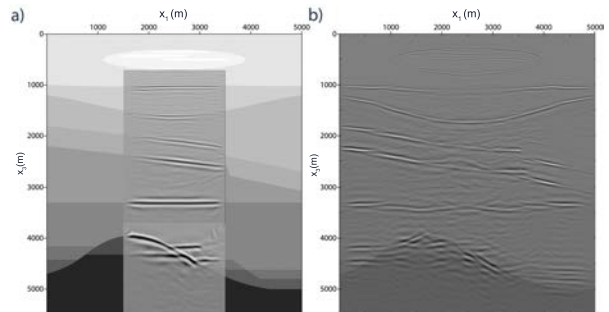


Figure 6: Migration images with a smooth velocity model. The background indicates the true model. a) Local image using the retrieved reflectivity as in Fig. 2 d) and 3 b). The polarity of the image from below is changed to be consistent with the surface image. b) Standard seismic image, obtained from data at the surface.

## Data-driven imaging above and below a horizontal well

### REFERENCES

- Bakulin, A., and R. Calvert, 2006, The virtual source method: Theory and case study: *Geophysics*, **71**, SI139 – SI150.
- Broggini, F., R. Snieder, and K. Wapenaar, 2012, Focusing the wavefield inside an unknown 1d medium: Beyond seismic interferometry: *Geophysics*, **77**, A25 – A28.
- Curtis, A., P. Gerstoft, H. Sato, R. Snieder, and K. Wapenaar, 2006, Seismic interferometry - turning noise into signal: *The Leading Edge*, **25**, 1082 – 1092.
- Curtis, A., and D. Halliday, 2010, Source-receiver wave field interferometry: *Phys. Rev. E*, **81**, no. 4, 046601.
- Galetti, E., and A. Curtis, 2012, Generalised receiver functions and seismic interferometry: *Tectonophysics*, **532535**, 1 – 26.
- Mehta, K., A. Bakulin, J. Sheiman, R. Calvert, and R. Snieder, 2007, Improving the virtual source method by wavefield separation: *Geophysics*, **72**, V79 – V86.
- Nakata, N., R. Snieder, T. Tsuji, K. Larner, and T. Matsuoka, 2011, Shear wave imaging from traffic noise using seismic interferometry by cross-coherence: *GEOPHYSICS*, **76**, SA97–SA106.
- Poletto, F., P. Corubolo, and P. Comelli, 2010, Drill-bit seismic interferometry with and without pilot signals: *Geophysical Prospecting*, **58**, 257 – 265.
- Poliannikov, O., 2011, Retrieving reflections by source-receiver wavefield interferometry: *Geophysics*, **76**, SA1–SA8.
- Schuster, G., J. Yu, J. Sheng, and J. Rickett, 2004, Interferometric/daylight seismic imaging: *Geophysical Journal International*, **157**, 838 – 852.
- Snieder, R., 2004, Extracting the green's function from the correlation of coda waves: A derivation based on stationary phase: *Phys. Rev. E*, **69**, no. 4, 046610.
- Snieder, R., M. Miyazawa, E. Slob, I. Vasconcelos, and K. Wapenaar, 2009, A comparison of strategies for seismic interferometry: *Surveys in Geophysics*, **30**, 503 – 523.
- Thorbecke, J., and D. Draganov, 2011, Finite-difference modeling experiments for seismic interferometry: *Geophysics*, **76**, H1–H18.
- van der Neut, J., J. Thorbecke, K. Mehta, E. Slob, and K. Wapenaar, 2011, Controlled-source interferometric redatuming by crosscorrelation and multidimensional deconvolution in elastic media: *Geophysics*, **76**, SA63 – SA76.
- van der Neut, J., and K. Wapenaar, 2015, Point-spread functions for interferometric imaging: *Geophysical Prospecting*.
- Vasconcelos, I., and R. Snieder, 2008a, Interferometry by deconvolution: Part 1 - Theory for acoustic waves and numerical examples: *Geophysics*, **73**, S115 – S128.
- , 2008b, Interferometry by deconvolution: Part 2 - Theory for elastic waves and application to drill-bit seismic imaging: *Geophysics*, **73**, S129 – S141.
- Wapenaar, K., F. Broggini, E. Slob, and R. Snieder, 2013, Three-dimensional single-sided Marchenko inverse scattering, data-driven focusing, Green's function retrieval, and their mutual relations: *Physical Review Letters*, **110**, 084301.
- Wapenaar, K., and J. Fokkema, 2006, Green's function representations for seismic interferometry: *Geophysics*, **71**, SI33 – SI46.
- Wapenaar, K., J. Thorbecke, J. van der Neut, F. Broggini, E. Slob, and R. Snieder, 2014, Marchenko imaging: *Geophysics*, **79**, WA39–WA57.
- Wapenaar, K., and J. van der Neut, 2010, A representation for Green's function retrieval by multidimensional deconvolution: *The Journal of the Acoustical Society of America*, **128**, EL366–EL371.
- Wapenaar, K., J. van der Neut, E. Ruigrok, D. Draganov, J. Hunziker, E. Slob, J. Thorbecke, and R. Snieder, 2011, Seismic interferometry by crosscorrelation and by multidimensional deconvolution: a systematic comparison: *Geophysical Journal International*, **185**, 1335 – 1364.